remote sensing

MDPI

Article

Annual Cropping Intensity Dynamics in China from 2001 to 2023

Jie Ren [1,*], Yang Shao [2] and Yufei Wang [3]

[1] School of Artificial Intelligence, Guilin University of Electronic Technology, Guilin 541004, China
[2] Department of Geography, College of Natural Resources and Environment, Virginia Tech, Blacksburg, VA 24061, USA; yshao@vt.edu
[3] School of Marine Science and Engineering, Nanjing Normal University, Nanjing 210023, China; yufeiw@njnu.edu.cn
* Correspondence: jieren@guet.edu.cn

Abstract: Spatial and temporal information about cropping patterns of single and multiple crops is important for monitoring crop production and land-use intensity. We used time-series MODIS NDVI 8-day composite data to develop annual cropping pattern products at a 250 m spatial resolution for China, covering the period from 2001 to 2023. To address the potential impacts of varying parameters in both data pre-processing and the peak detection algorithm on the accuracy of cropping pattern mapping, we employed a grid-search method to fine-tune these parameters. This process focused on optimizing the Savitzky–Golay smoothing window size and the peak width parameters using a calibration dataset. The results highlighted that an optimal combination of a five to seven MODIS composite window size in Savitzky–Golay smoothing and a peak width of four MODIS composites achieved good overall mapping accuracy. Pixel-wise accuracy assessments were conducted for the selected mapping years of 2001, 2011, and 2021. Overall accuracies were between 89.7% and 92.0%, with F1 scores ranging from 0.921 to 0.943. Nationally, this study observed a fluctuating trend in multiple cropping percentages, with a notable increase after 2013, suggesting shifts toward more intensive agricultural practices in recent years. At a finer spatial scale, the combination of Mann–Kendall and Sen's slope analyses revealed that approximately 12.9% of 3 km analytical windows exhibited significant changes in cropping intensity. We observed spatial clusters of increasing and decreasing crop intensity trends across provinces such as Hebei, Shandong, Shaanxi, and Gansu. This study underscores the importance of data smoothing and peak detection methods in analyzing high temporal resolution remote sensing data. The generation of annual single/multiple cropping pattern maps at a 250 m spatial resolution enhances our comprehension of agricultural dynamics through time and across different regions.

Keywords: cropping intensity; time-series analysis; peak detection; MODIS

check for updates

Citation: Ren, J.; Shao, Y.; Wang, Y. Annual Cropping Intensity Dynamics in China from 2001 to 2023. *Remote Sens.* **2024**, *16*, 4801. https://doi.org/10.3390/rs16244801

Academic Editor: Dino Ienco

Received: 20 November 2024
Revised: 20 December 2024
Accepted: 21 December 2024
Published: 23 December 2024

Copyright: © 2024 by the authors. Licensee MDPI, Basel, Switzerland. This article is an open access article distributed under the terms and conditions of the Creative Commons Attribution (CC BY) license (https://creativecommons.org/licenses/by/4.0/).

1. Introduction

Double or multiple cropping is a key method for increasing grain output [1,2] and it is also a widely used management strategy for crop diversification [3], risk-spreading [4], and coupled economic–environmental benefits [5,6]. In China, multiple cropping contributes to roughly 33% of the nation's total grain output, marking it as an essential element of the Chinese agricultural ecosystem [7,8]. Understanding the spatial and temporal aspects of multiple cropping is crucial for assessing crop productivity, identifying cropping patterns, and shaping agricultural policies. The urgency for such insights is accentuated by China's fast urbanization and the ensuing alterations in agricultural land use, particularly the marginalization or abandonment of croplands and a potential trend toward transitioning from multiple to single cropping systems [9,10].

Time-series remote sensing data have been extensively used for identifying crop types, understanding crop phenology, documenting crop rotations, and tracking their changes or trends [11–14]. Despite the broad application of such data across various

agricultural monitoring objectives, there has been relatively less research focused on the mapping of single or multiple cropping patterns, particularly at a national scale in countries like China and spanning long durations. Zhu et al. [15] conducted mapping of single and double cropping systems at a 1 km spatial resolution using 10-day Maximum Value Composite SPOT/VGT Normalized Difference Vegetation Index (NDVI) time-series for the northern provinces of China from 1999 to 2004. Subsequent studies have enhanced the mapping resolution to 500 m using Moderate Resolution Imaging Spectroradiometer (MODIS) data [16,17]. Liu et al. [18] developed 250 m global annual cropping intensity products for the years 2001–2019 using MODIS Enhanced Vegetation Index (EVI), marking significant progress in the spatial resolution of agricultural mapping.

Identifying trends in single and multiple cropping patterns typically requires detailed, long-term analysis on a pixel-by-pixel basis. The complexity of this task is due to the ever-changing agricultural practices and environmental conditions. For earlier studies, data accessibility issues arose as map products may not have been publicly available. More recent mapping products are still difficult to compile due to differences in spatial resolution, the time periods covered, and the high level of uncertainties in mapping accuracy. For instance, we conducted a quick comparison of the two most recent studies by Qiu et al. [16] and Liu et al. [18], specifically examining the crop intensity maps for China from 2015–2021. We found that the average percentage of single cropping within total croplands was approximately 64% and 84%, respectively, according to these studies. Such a discrepancy highlights the considerable uncertainty inherent in remote sensing-derived cropping patterns. Further research is necessary to enhance the accuracy of mapping algorithms and the integration of diverse data sources, such as cropland masking, as well as to validate remote sensing-derived cropping maps with ground-truth data.

Mapping single or multiple cropping patterns encounters challenges similar to those found in other time-series remote sensing applications. Specifically, mapping results are sensitive to various analytical components, including the spatial–temporal resolution of input data, image noise, and specific algorithms used for single/multiple cropping detection. For instance, time-series data smoothing algorithms such as Savitzky–Golay, Whittaker smoother, and Harmonic Analysis are commonly used in the first step to remove data noise within the time-series; subsequent peak detecting algorithms are then combined with certain decision rules to map out single or multiple crops for each pixel [15–19]. It is unclear how certain smooth parameters, for example, the window size in the Savitzky–Golay (SG) approach, are selected. Similarly, researchers may need to adjust various rules or parameters in peak detection of the time-series data. There is a pressing need to investigate methodologies that integrate detailed calibration of these parameters in supporting automated single/multiple cropping mapping.

The research objectives of this study were twofold: firstly, to develop 250 m resolution, national-scale mapping products of single and multiple cropping patterns in China, covering the period from 2001 to 2023; and secondly, to analyze the spatial and temporal trends of these cropping patterns. Our approach involved using 250 m MODIS time-series data to produce accurate and consistent maps of single and multiple cropping practices. Initially, we focused on determining the critical parameters for data smoothing and peak detection algorithms. This involved employing a grid-search method to fine-tune the mapping performance based on a calibration dataset. The optimized parameters were then applied to the entire dataset to create annual maps of single and multiple cropping patterns. Subsequently, we conducted an analysis of the temporal trends in cropping patterns to understand whether there have been significant changes over the study period. Identifying regions that exhibit substantial shifts in cropping practices was a key aspect of this analysis. This research aimed to provide essential data that can support informed decision-making at both the regional and national levels, ultimately contributing to improved agricultural productivity and enhanced food security.

2. Materials and Methods

2.1. Data and Data Preprocessing

The MODIS/Terra Surface Reflectance 8-Day data (MOD09Q1) spanning the years 2001–2023 were acquired from NASA's Earthdata Search (https://search.earthdata.nasa.gov/, accessed on 1 January 2024). Among available satellite datasets, MODIS is particularly valuable for time-series analysis due to its high temporal resolution (1–2 days). The 8-day and 16-day MODIS composite data effectively reduce cloud cover impacts present in the original daily data, making it widely used in agricultural mapping. Compared to Landsat or Sentinel datasets, MODIS time-series data is well-suited for national and global mapping because it provides a long time span (2000 to the present), an intermediate spatial resolution of 250 m, and frequent temporal coverage. To encompass the study area as illustrated in Figure 1, 19 MODIS tiles from horizontal zones 23 to 29 and vertical zones 3 to 7 were selected, resulting in a total of 20,102 MODIS tiles gathered for the analysis. We extracted surface reflectance values for Band 1 (Red) and Band 2 (near-infrared, NIR) for calculating the NDVI. NDVI mosaics were generated for every 8-day composite period. These mosaics were then re-projected to the Albers Equal Area Conic (AEA) projection system using a nearest-neighbor resampling method. The resolution of the NDVI data is 250 m × 250 m per grid cell.

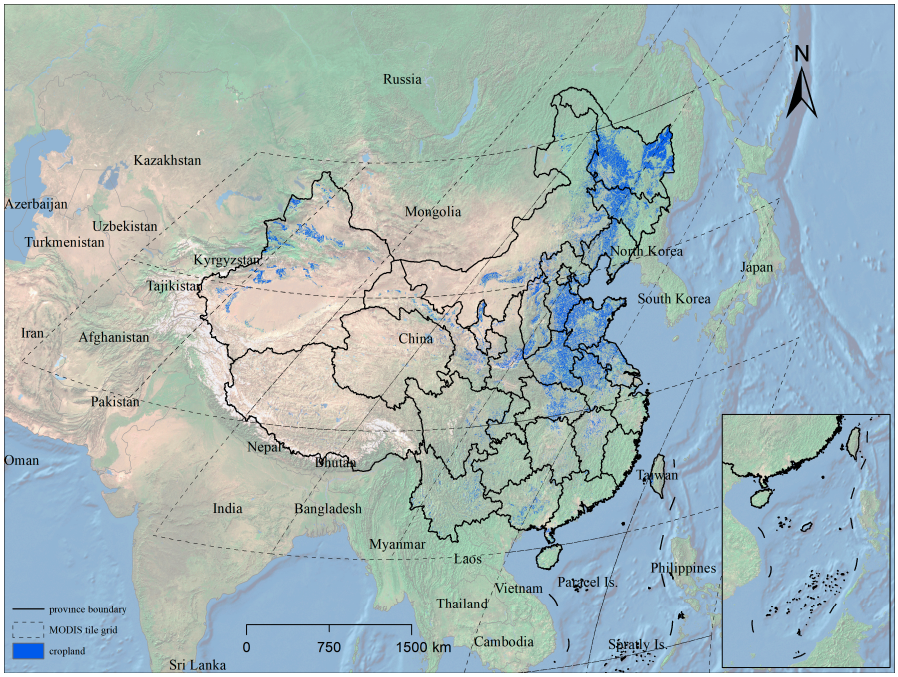

Figure 1. MODIS tiles (represented by dashed-line polygons) spanning horizontal zones 23 to 29 and vertical zones three to seven. Cropland distribution at a 250 m resolution. The 10 m land cover map products were employed to determine the percentage of croplands.

Cropland mask was derived from the 10 m land use and land cover map [20]. These land cover map products were derived from Sentinel-2 images using deep learning algorithms. The ESRI land cover map has an overall accuracy of 85.96% [20]) and the cropland/non-cropland specific accuracy was 85.33% [21]. The original 9-class map products for 2022 were downloaded from https://livingatlas.arcgis.com/landcover/, accessed on 10 July 2024. We singled out the cropland class and computed proportions within each 250 m MODIS grid cell. For the purpose of mapping single or multiple cropping patterns, only MODIS pixels where the cropland proportion exceeded 90% were selected. The overall distribution of 'pure' cropland pixels is illustrated in Figure 1.

To support our cropping pattern mapping task, we leveraged the crop intensity map products from Qiu et al. [16] covering the years 2015 to 2021, creating a calibration

dataset. Their processing code and related files are available at https://doi.org/10.6084/m9.figshare.14936052, accessed on 18 September 2024. We randomly selected 5000 pixels that consistently exhibited either single or multiple cropping patterns over the seven-year span. From this selection, a smaller subset (n = 1000) from the initial set of 5000 pixels was visually analyzed using corresponding NDVI time-series data, confirming an overall accuracy exceeding 90%. Utilizing this set of calibration data allowed us to assess various methods for mapping cropping patterns and to fine-tune parameters for improved mapping accuracy. Preliminary testing also showed that reducing the sample size to 1000 or expanding it to 20,000 had minimal impact on the analysis results after reaching 3000 sample pixels.

2.2. Data Smoothing

The original NDVI time series derived from the MODIS data contains noise, characterized by spikes and dips due to cloud cover, shadows, weather conditions, and noise introduced by the sensor itself [22]. We applied the widely recognized Savitzky–Golay (SG) smoothing to reduce image noise [23]. The SG method employs a sliding window across the dataset, where a polynomial of second degree is fitted to the data points within each window (e.g., 2n + 1 points, with n being the window size chosen by the user). The value at the center of each window is substituted with the value derived from the polynomial fit. For a given application, the ideal window size is unknown, necessitating a careful selection process to balance the trade-offs between smoothing the data sufficiently to remove noise while preserving the true signal, especially the important features of the NDVI time series such as seasonal peaks. We implemented this process using the TIMESAT software package [24]. We noted that TIMESAT smoothing algorithms typically require approximately 75% of valid data points within a time series to accurately predict realistic values for missing data [25]. Using the MODIS QA layers as input, we identified pixels labelled as cloudy or in a shadow state. We then assessed the annual NDVI time series and flagged locations with more than 25% missing values (i.e., cloud or shadow). For each mapping year from 2001 to 2023, we generated a quality layer, labeling pixels with more than 25% missing data as 0 and those with less than 25% missing data as 1. For pixels coded as 1, we examined the presence of single or multiple cropping patterns by analyzing the number of peaks within each calendar year, using the reconstructed NDVI time series.

2.3. Peak Detection

While earlier research differentiated between double and triple cropping within the multi-cropping framework, triple cropping accounts for only about 0.33–2% of the total cropland area [8,26]. For simplicity, we grouped double and triple cropping practices together under a broader category of multiple cropping. We used the "findpeaks" function from MATLAB R2002a's signal processing toolbox for peak detection. Figure 2 presents NDVI signal examples for both single and double cropping scenarios, displaying data from one year for clarity. We employed a threshold of 0.35 for NDVI values [18], considering only those above this threshold as potential peak candidates. In the case of single cropping, a single NDVI peak indicates one primary growing season. For identifying multiple cropping patterns, we adopted an additional criterion that requires at least 80 days between peaks, following the guidelines established by Sakamoto et al. [27] and Yang et al. [28]. The findpeaks function automatically selects the tallest peak in the NDVI time-series and removes peaks that occur within 10 consecutive 8-day MODIS composite periods. This process is iteratively repeated through the built-in feature.

Using the aforementioned calibration data as a basis, we carefully analyzed the peak detection results and their connection to single and multiple cropping systems. For certain time-series, we identified smaller peaks that did not correspond to actual crop growing seasons. To improve our peak detection techniques, we evaluated additional criteria such as peak width and prominence, as illustrated in Figure 2. Peak width is important as it directly corresponds to the crop growing cycle while peak prominence has a lesser impact on improving the accuracy of distinguishing between single and multiple cropping. For

example, a peak width of more than 30 days (equivalent to approximately four 8-day MODIS composites) was found to be necessary to represent a crop growth cycle, ensuring the NDVI signal accurately reflects the phenological stages of crop development. The calibration data facilitated the examination of various peak widths to identify the optimal settings for accurate crop cycle representation.

Concurrently, we examined how the SG smoothing technique influences peak detection, mainly by adjusting the size of the smoothing window (ranging from 5 to 13 in increments of 2) and adjusting the peak width (ranging from 2 to 6.5 in increments of 0.5). This process aimed to assess their effect on accurately identifying single or multiple cropping patterns. We employed a grid search method to pinpoint the best combination of parameters by matching detected peaks against known cropping patterns of either single or multiple cycles. The effectiveness of each set of parameters was quantitatively assessed using the F1 score [29], a commonly used measure of mapping accuracy. The F1 score provides a balance between precision and recall, which is essential for handling potential imbalances between cropping categories. The parameter set that achieved the highest F1 score was then applied in mapping cropping patterns for all cropland pixels over a period from 2001 to 2023.

Accuracy assessments were carried out pixel-wise for specific mapping years: 2001, 2011, and 2021. For each year's map, 350 pixels (about 0.04‰ of total cropland pixel) were randomly chosen to verify the identification of single or multiple cropping patterns, totaling 1050 random points for the overall accuracy evaluation. MODIS 8-day time-series data were used as a reference in a visual assessment to record the number of peaks. The accuracy of the mapping was quantified using confusion matrix, overall accuracy, and the F1 score.

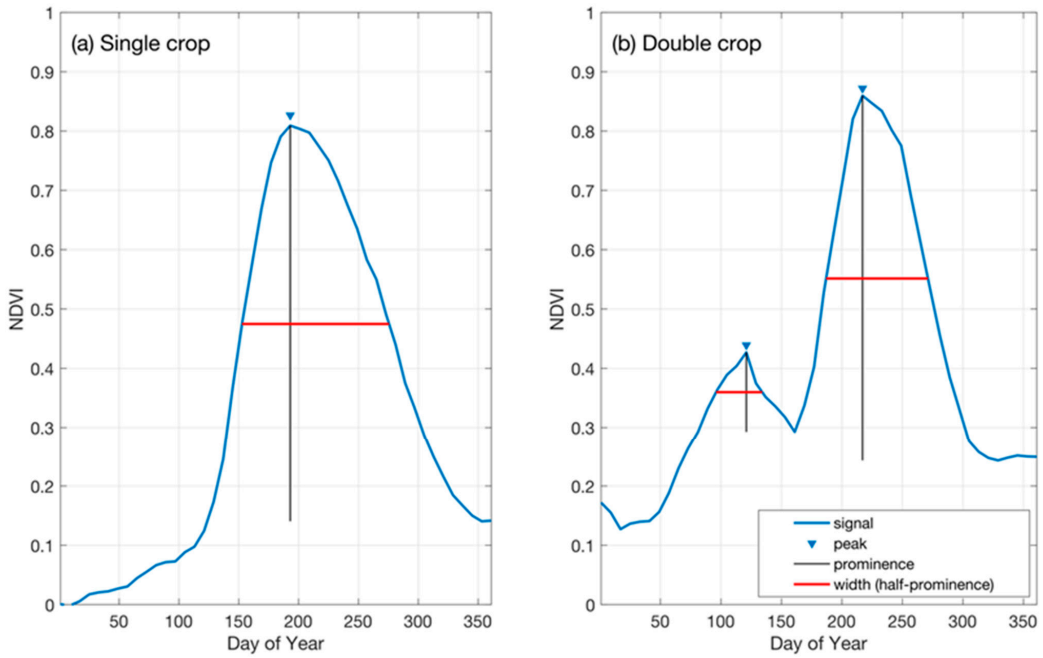

Figure 2. Illustration of time-series NDVI data in 2023 for single crop (**a**) and double crop (**b**). Peak width at half-prominence is highlighted in red.

2.4. Trend Analysis of Cropping Patterns

The annual single/multiple crop mapping results from 2001 to 2023 were used to support the long-term crop intensity change analysis. For each mapping year, single and multiple cropping patterns were encoded as 1 and 2, respectively, for each 250 m MODIS pixel. To approximate crop intensity, average values were computed within 3 km by 3 km moving windows. Long-term trends in crop intensity from 2001 to 2023 were then analyzed on a window-by-window basis using the non-parametric Mann–Kendall test, which is well-

suited for environmental data as it does not assume a specific distribution. For 3 km × 3 km grids with significant trends, Sen's slope estimator was applied to determine the direction and magnitude of these trends. Positive or negative trends in crop intensity were identified based on Sen's slope results, highlighting areas with significant increases or decreases in cropping intensity over the 23-year period. This approach allowed us to pinpoint specific areas where crop intensities were either rising or declining.

2.5. Mapping Implementation and Computational Design

Processing the extensive dataset of 20,102 8-day MODIS scenes covering the period from 2001 to 2023, along with the associated data preprocessing tasks such as applying the SG smoothing and employing the findpeaks function, required substantial computing resources. To enhance efficiency, we adopted a parallel processing strategy, leveraging the Tinkercliffs cluster through Virginia Tech's Advanced Research Computing (ARC) services. Spatially, cropland pixels were segmented into smaller processing groups, while temporally, MODIS time-series data were broken down into more manageable segments, allowing functions like findpeaks to be executed on an annual basis. The data and workflow to produce an annual cropping intensity map are shown in Figure 3.

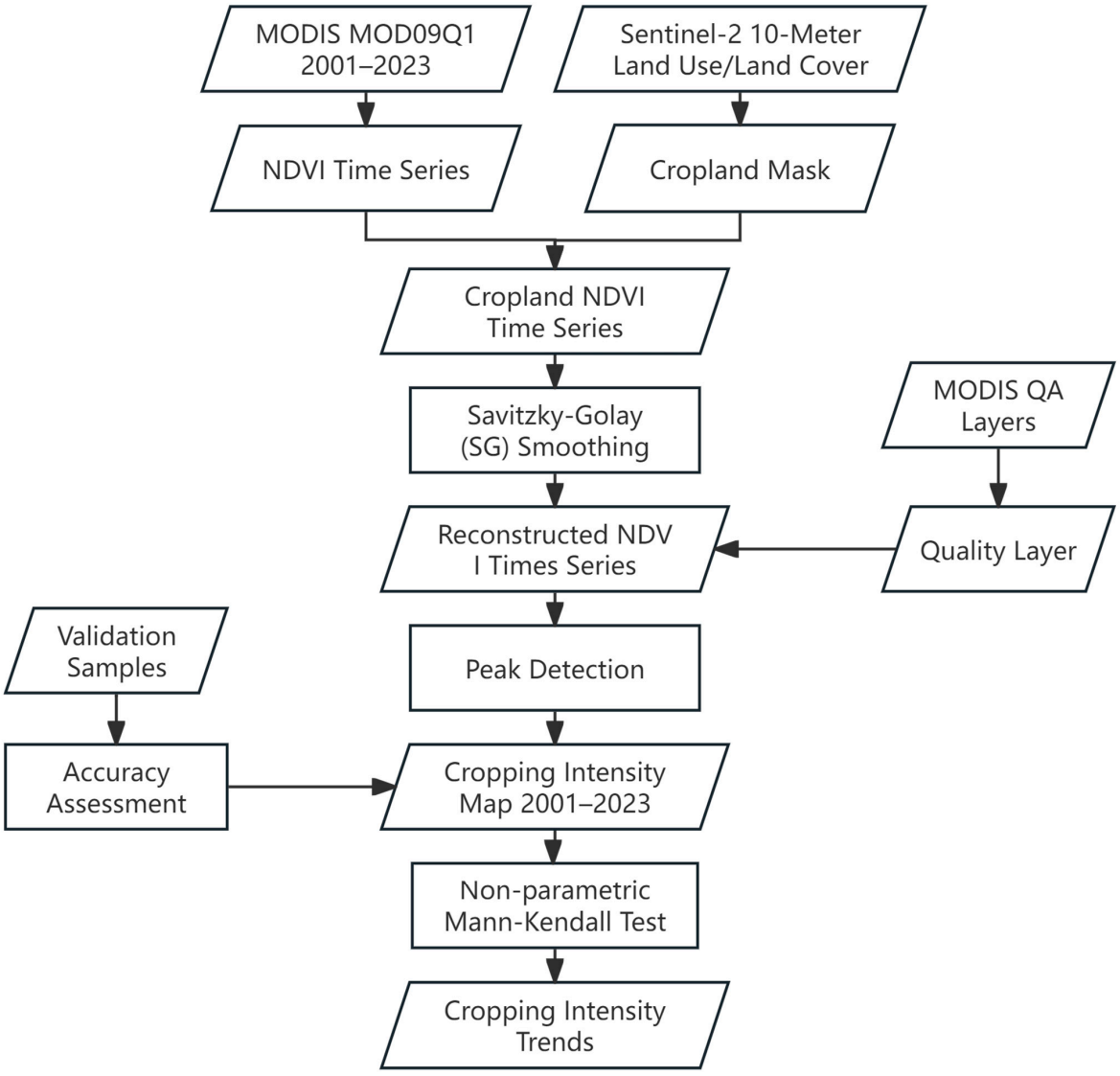

Figure 3. Data and workflow for cropping intensity mapping.

3. Results

3.1. Impacts of Data Smoothing and Peak Detection Parameters

We used the F1 scores to evaluate the accuracy of single/multiple crop mapping for the calibration dataset (n = 5000). A higher F1 score (i.e., closer to 1) indicates higher accuracy. It is important to mention that we implemented two threshold criteria to detect NDVI peaks: a minimum NDVI value of 0.35 and a minimum interval of 80 days between consecutive peaks. Figure 4 illustrates how applying additional thresholds and parameters, such as SG window sizes and peak widths, affects F1 score variations.

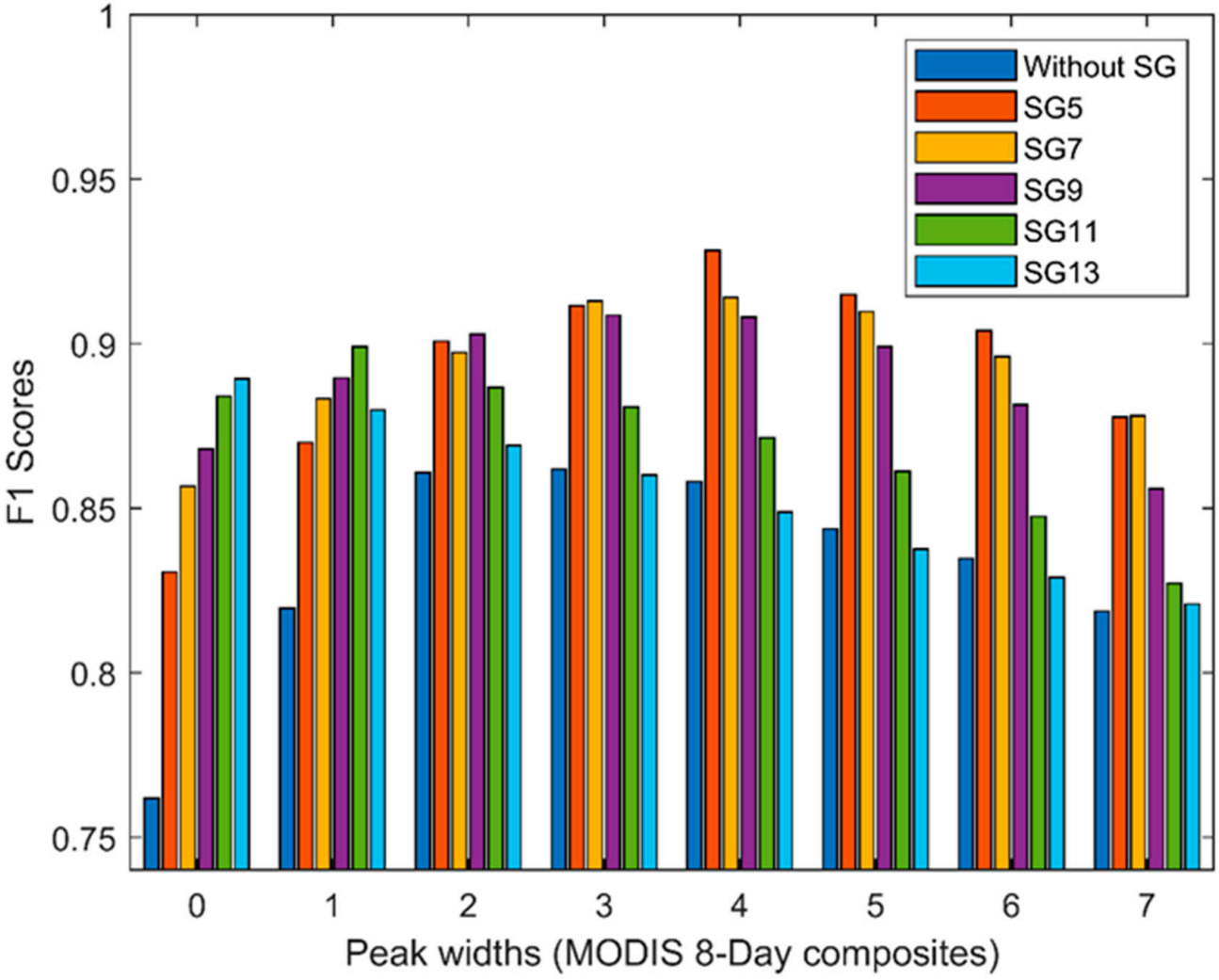

Figure 4. Comparison of F1 scores across different peak detection methods, examining the impact of various Savitzky–Golay (SG) smoothing combinations, SG window sizes, and peak width parameters.

The application of the SG smoothing generally enhanced the accuracy of peak detection and mapping. For instance, when the peak width criterion was omitted (i.e., peak width set to 0), the F1 score obtained using the original NDVI time series as input was 0.762. However, when employing SG filtering with window sizes ranging from 5 to 13 for 8-day MODIS composites, the F1 scores notably improved, falling between 0.831 and 0.889. This improvement underscores the importance of data denoising. The presence of abrupt increases and decreases in the original NDVI time series complicates its direct use for accurate peak detection or the mapping of cropping patterns.

For SG filter window sizes ranging from five to eleven on MODIS composites, F1 scores increased and then decreased as the peak width criterion was adjusted from zero to seven. The optimal F1 scores were achieved with a peak width threshold of three to four

MODIS composites (equivalent to 24–32 days). Peaks with a duration shorter than 24 days typically do not reflect genuine crop growth cycles. Utilizing an excessively broad peak width threshold, such as seven 8-day MODIS composites, poses the risk of overlooking narrower peaks. This oversight could result in the misclassification of areas with multiple cropping cycles as having only a single crop cycle. Moreover, employing wider SG filter window sizes, such as 13, resulted in diminished peak detection accuracy compared to the outcomes from narrower window sizes. This drop in accuracy was particularly notable when broader peak width criteria were applied.

The optimal parameter combination, yielding the highest F1 score of 0.928, involved an SG moving window size of five and a peak width of four. These calibrated parameters were applied to map single/multiple cropping patterns across all cropland areas from 2001 to 2023.

3.2. Annual Cropping Pattern Maps and Accuracy Assessment

Accuracy assessment of single/multiple cropping was evaluated on a pixel-by-pixel basis at a 250 m resolution for selected mapping years of 2001, 2011, and 2021. As depicted in Table 1, the overall accuracy ranged from 89.7% to 92.0%, and corresponding F1 scores 0.921 to 0.943. These F1 scores align closely with those derived from the training dataset, indicating robust model performance. The user accuracy (UA) for single crop classifications was high, above 94% for all three mapping years. The UA for multiple crop classifications were lower, ranged from 81.9% to 84.4%. A closer examination of NDVI time series data for misclassifications of multiple crops suggested that they predominantly occurred in the southern provinces. This issue is largely attributed to the increased levels of uncertainty in NDVI time-series data caused by cloud cover and rain, which are more prevalent in these regions.

Table 1. Pixel-wise (250 m) accuracy assessment for the 2001, 2011, and 2021 cropping pattern mapping.

	Reference					
	2001		2011		2021	
	SC	MC	SC	MC	SC	MC
SC	210	13	230	11	216	13
MC	23	104	17	92	20	101
OA (F1)	89.7 (0.921)		92.0 (0.943)		90.6 (0.929)	
SC	UA: 94.2	PA: 90.1	UA: 95.4	PA: 93.1	UA: 94.3	PA: 91.5
MC	UA: 81.9	PA: 88.9	UA: 84.4	PA: 89.3	UA: 83.5	PA: 88.6

SC: Single crop; MC: Multiple crop; OA: Overall accuracy; UA: User's accuracy; PA: Producer's accuracy.

The spatial distributions of single/multiple crops are depicted in Figure 5. To simplify the visualization, only the map for 2023 is displayed. Areas with a concentration of multiple cropping practices include the provinces of Henan, Shandong, Hebei, Anhui, and Jiangsu (Figure 5c,d). As reported in Chen et al. [30], the varieties of multiple cropping systems vary by region. For instance, the provinces of Henan, Shandong, and Hebei are predominantly characterized by wheat–corn double cropping patterns. In contrast, Anhui and Jiangsu are primarily associated with wheat–rice double cropping systems. Single cropping systems are predominantly found in the northern and northwestern regions of China, including the provinces of Heilongjiang, Jilin, Liaoning, the Inner Mongolia Autonomous Region, Gansu Province, and certain areas of the Xinjiang Uygur Autonomous Region (Figure 5a,b). This prevalence is attributed to the region's climatic conditions, which feature a colder climate and shorter growing season in comparison to the more temperate and subtropical areas of China.

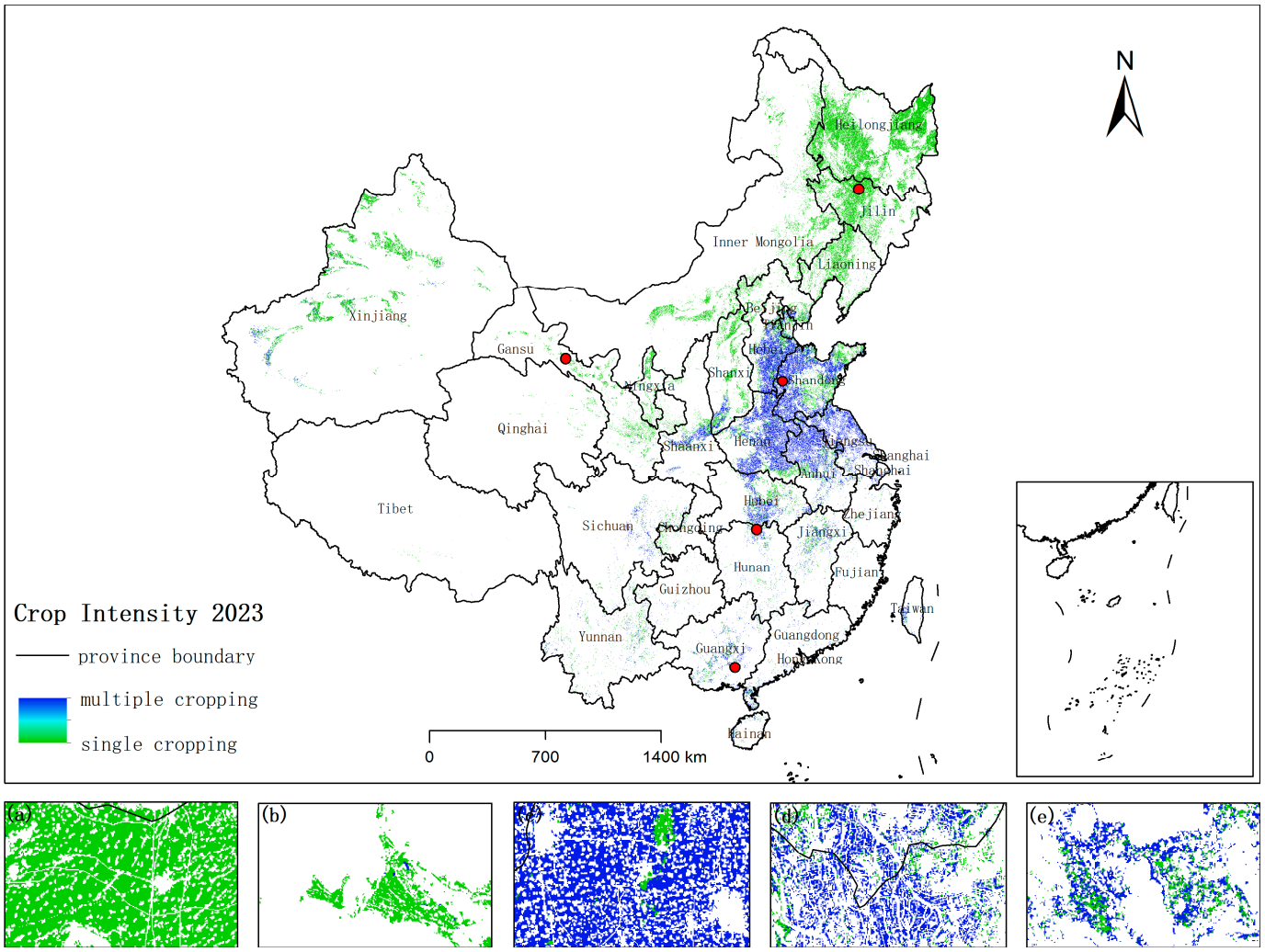

Figure 5. MODIS-derived map of single and multiple cropping patterns for the year 2023. The subplots show the details of the cropping intensity within major agricultural regions in China and their locations are indicated by red dots: (**a**) Northeast China Plain, (**b**) Qinghai-Tibet Plateau, (**c**) North China Plain, (**d**) Yangtze Plain, and (**e**) Southern China. Only the 2023 map is presented here for simplicity.

3.3. Trend Analysis of Cropping Intensity

At the national level, the percentages of multiple crops within all cropland from the year 2001 to 2023 are depicted in Figure 6. The percentages ranged from 29.6% to 35.2%. Generally, there was a decline from 2001, reaching the lowest point around 2013. From 2013 onward, there was an upward trend with fluctuations, suggesting a shift toward more intensive agricultural practices over the recent period. Toward the latter part of the timeline, the percentage approached some of the higher levels observed (~34%) within the series, yet it remained marginally below the initial levels recorded in 2001.

The analysis of crop intensity at a local level was conducted through the examination of 3 km × 3 km analytical windows, with trend analysis of 268,350 windows, each incorporating at least one 250 m cropland pixel. Approximately 14.5% of these windows displayed significant trends ($p < 0.05$) according to the Mann–Kendall test, indicating monotonic changes in cropping patterns between 2001 and 2023. Additional Sen's slope analysis pinpointed that a specific subset of these windows (n = 34,569 or roughly 12.9%) showed either positive or negative changes.

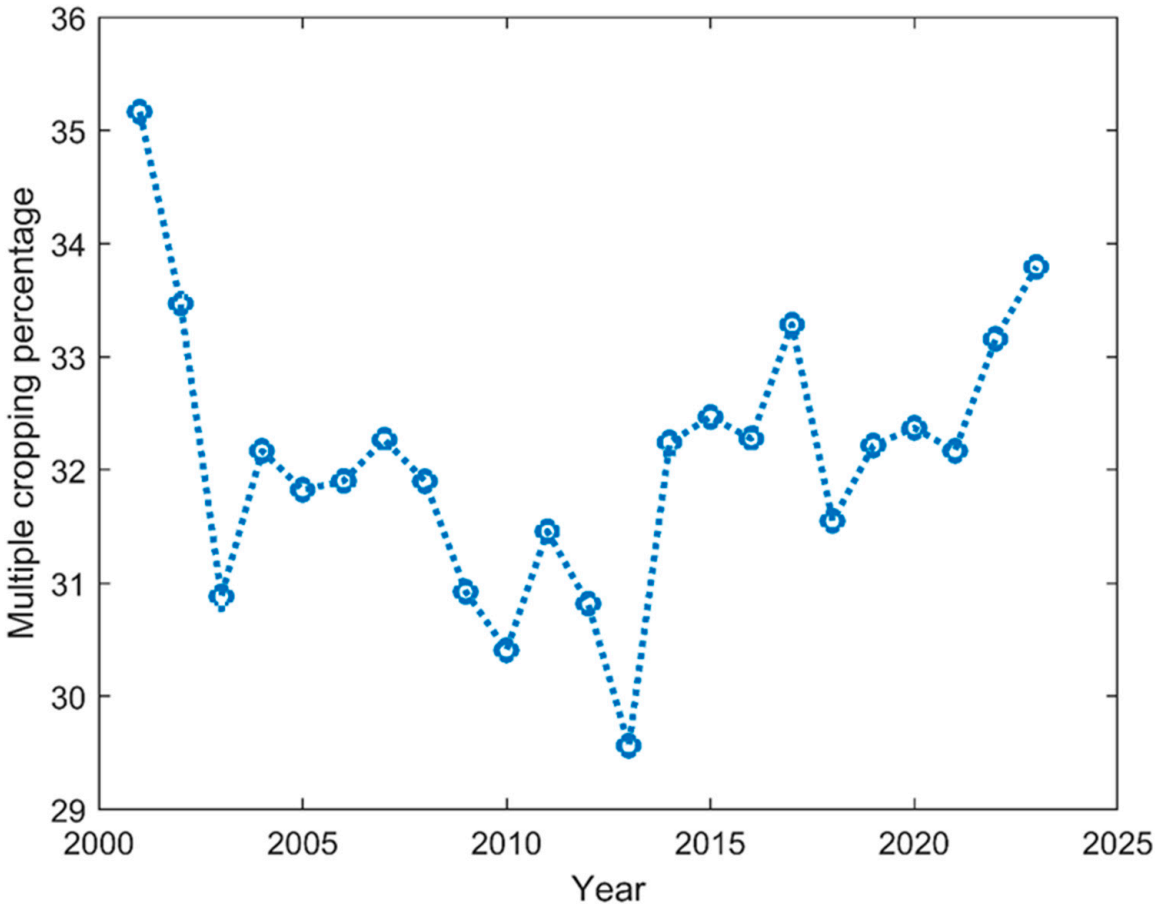

Figure 6. The percentages of multiple crops within all cropland from the year 2001 to 2023.

Figure 7 shows the locations where significant shifts in crop intensity have been quantitatively identified using the Mann–Kendall test and Sen's slope. Notably, about half of these highlighted areas exhibited upward trends, suggesting an increase in crop intensity over the observed period. Such upward trends were particularly prominent in clusters located within the Hebei and Shandong Provinces. Conversely, a noticeable decrease in crop intensity was observed in Shaanxi and Gansu Provinces. These findings underscore the spatial variability of agricultural intensification and retreat, offering insights into regional agricultural dynamics. Figure 8 offers further analysis on changes in cropping intensity, highlighting NDVI time-series data from 2001 to 2023 for two selected 3 km sample windows. Figure 8a illustrates the transition from multiple to single cropping practices, and Figure 8b shows the shift from single to multiple cropping practices. The Sen's slope values for these two windows are −0.0245 and 0.0279, respectively, indicating decreasing and increasing trends in cropping intensity. For these sample windows, average NDVI values were computed for all cropland pixels within each window across each MODIS composite.

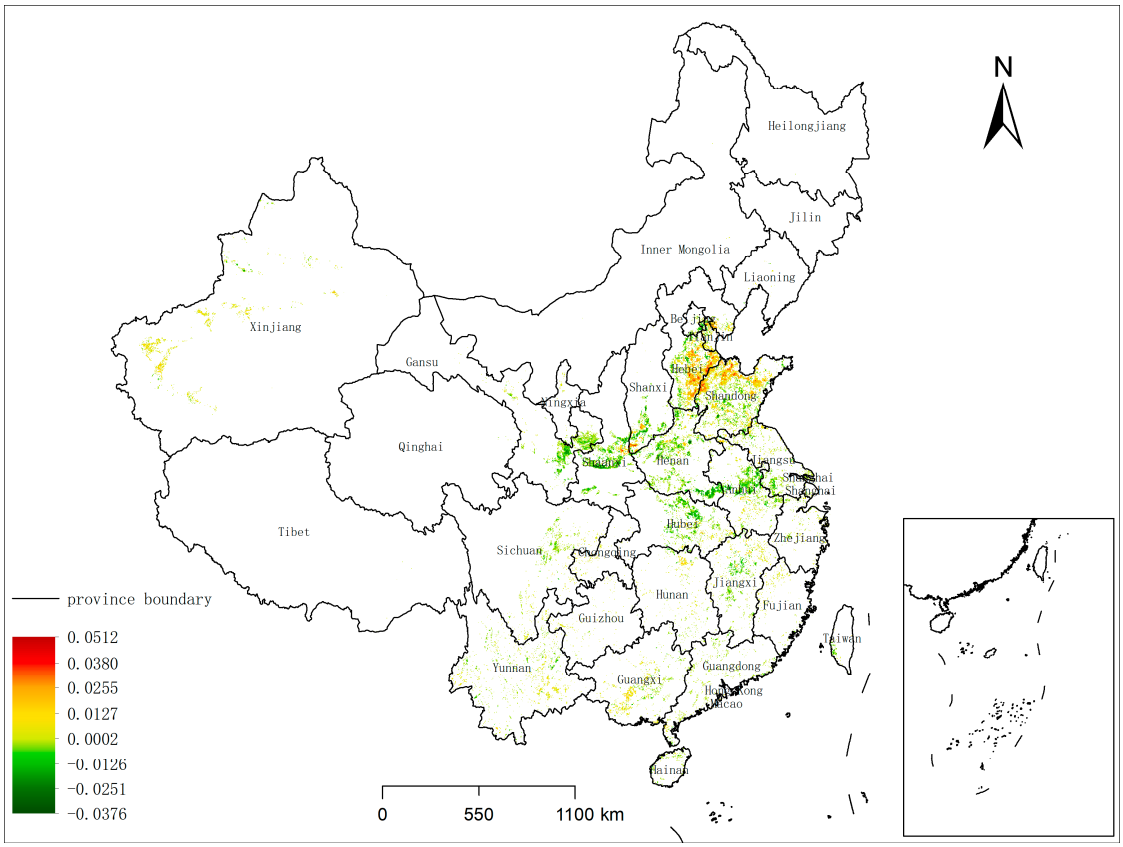

Figure 7. Slope coefficient (change rate) of cropping intensity trend model (2001–2023). Note only 3 km windows showing significant ($p < 0.05$) upward/downward trends based on the Mann–Kendall test were used for trend model development.

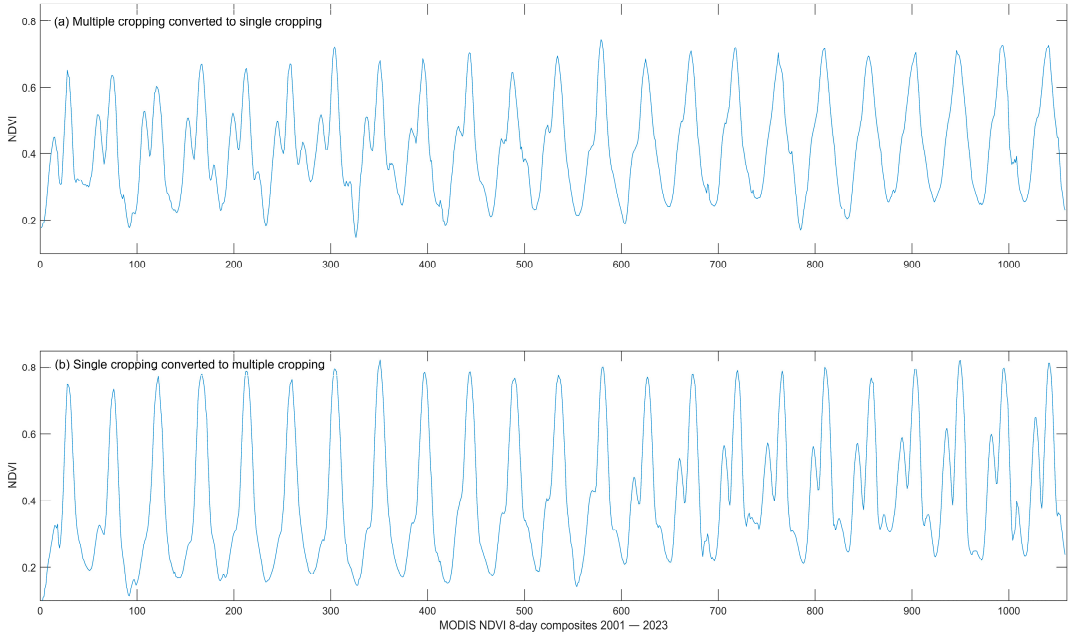

Figure 8. NDVI time series from 2001 to 2023 for two selected 3 km analytical windows: (**a**) areas transitioning from multiple to single cropping practices, and (**b**) areas transitioning from single to multiple cropping practices. NDVI values were averaged for all cropland pixels within each 3 km window for every MODIS composite.

4. Discussion

Our cropping pattern mapping started with the application of two threshold criteria for NDVI peak detection: a baseline NDVI value of 0.35 and a minimum 80-day interval between successive peaks. Data smoothing techniques, specifically the SG smoother, proved essential for eliminating spurious fluctuations, with smaller moving window sizes (five to seven MODIS composites) being particularly effective. Overly aggressive smoothing of NDVI time-series data may adversely affect peak detection and the accurate mapping of cropping patterns. Similar results were reported in other studies focusing on the impacts of data smoothing on land cover mapping [22].

Different from previous studies, we incorporated an additional peak width threshold to effectively exclude 'narrow' peaks that do not correspond to the crop-growing cycle. Again, there was no prior knowledge on the choice of threshold. Our key optimization step involved utilizing comprehensive training data, enabling the simultaneous fine-tuning of data smoothing and peak detection parameters. Despite the potential challenges and time required to gather such data [15], we believe that it should be an essential initial step in most remote sensing-based cropping pattern mapping tasks. Without a good calibration dataset and optimized mapping algorithms, achieving accurate and reliable mapping of cropping patterns over extended periods would be significantly hindered.

In addition to conducting pixel-wise accuracy assessments, we explored other cropping intensity map products to further validate our mapping results. We note that many available cropping intensity products differ in temporal and spatial resolutions, as well as in the cropland masks applied. We compared our results with GCI30, a global 30 m cropping intensity mapping product developed by Zhang et al. [30]. We selected GCI30 due to its higher spatial resolution (30 m) and strong overall accuracy (above 90%). GCI30 was derived using a combination of Landsat 7 ETM+, Landsat 8 OLI, and Sentinel-2 MSI imagery, with MODIS Vegetation Index (MOD13Q1) data used for gap-filling purposes. The dataset represents a single-layer cropping pattern averaged over a three-year window (2016–2018). We also introduced the GCI250 dataset by Liu et al. [17] for comparison, as it shares the same spatial resolution (250 m) and similar temporal coverage (2001–2019) as our dataset. GCI250 was derived using the Enhanced Vegetation Index (EVI) from MOD13Q1 data, processed through a sixth-order polynomial function. Table 2 compares the proportions of single and multiple cropping areas across the datasets. For consistency, the proportions in GCI250 and our data products were averaged over the period 2016–2018 to align with the GCI30 dataset. Among the datasets, GCI250 exhibited the highest proportion of single cropping (82.8%). The proportions of single cropping in GCI30 and our dataset were 74.9% and 67.6%, respectively. Spatially, the comparison between GCI30 and our results revealed a more consistent pattern of single and multiple cropping across China. In contrast, GCI250 tended to overestimate single cropping and underestimate multiple cropping.

Table 2. Proportions of single and multiple cropping intensity in China from different studies.

Existing Products and Studies	Study Period	Spatial Resolution	Single Cropping Area (%) (2016–2018)	Multiple Cropping Area (%) (2016–2018)	MCI of China
GCI30 [29]	2016–2018	30 m	74.9	25.1	1.25
GCI250 [17]	2001–2019	250 m	82.8	17.2	1.17
Our study	2001–2023	250 m	67.6	32.4	1.32

To enable pixel-wise comparisons, we aggregated the 30 m resolution GCI30 dataset to 250 m to align with the MODIS-derived cropping patterns. Both the GCI250 and our dataset were averaged over the 2016–2018 period using a voting approach. To mitigate inconsistencies, we excluded mismatched areas caused by differing cropland masks and missing data across the three datasets. For the remaining consistent cropland extent, we compared our dataset and GCI250 against the aggregated GCI30, used as a reference

(ground truth). The overall agreement between our dataset and GCI30 was 92%, while the agreement between GCI250 and GCI30 was 88%. These results indicate that our MODIS-derived 250 m cropping pattern aligns well with the high-resolution GCI30 dataset, demonstrating the robustness of our mapping approach.

The observed differences in cropping patterns can largely be attributed to the cropland masks used in these studies. Zhang et al. [31] integrated ten existing land cover maps to identify common cropland pixels for the development of GCI30. In contrast, Liu et al. [18] employed the Self-adapting Statistics Allocation Model of Global Cropland (SASAM-GC) [32] and used probabilities greater than 10% cropland as the mask for GCI250. This approach likely led to the inclusion of more cropland pixels with mixed signals from non-cropland land cover types, which may explain the high percentage (82.8%) of single-cropping patterns identified in their products. In our study, we utilized ESRI's 10 m land cover product to identify relatively pure cropland pixels by applying a 90% threshold within each 250 m grid. Consequently, our cropping pattern can be considered more representative of actual cropland use, minimizing the influence of mixed signals from non-cropland cover types.

Within the common cropland mask used across these three products, differences in single and multiple cropping patterns were driven by the mapping algorithms. Zhang et al. [31] relied on detecting transition points within time-series data, whereas our approach focused on peak detection combined with peak width thresholding. Liu et al. [18] used a sixth-order polynomial fitting method to map cropping intensity. Each of these methods has its own strengths and weaknesses, although a pixel-wise comparison showed better agreement between our data and GCI30.

Our study provides valuable insights into the spatial and temporal dynamics of single and multiple cropping patterns in China from 2001 to 2023. The combined use of the Mann–Kendall test and Sen's slope analysis underscores the changes occurring within China's agricultural landscape. Our findings reveal a fluctuating yet generally increasing trend in multiple cropping practices over the observed period, particularly post-2010. This resurgence may signify a strategic response to enhancing food security and optimizing land use efficiency amidst the pressures of urbanization and climate change [33–35]. The pronounced clusters of increased crop intensity in Hebei and Shandong provinces, as identified in our analyses, suggest regional hotspots of agricultural intensification that may be driven by favorable policies, technological advancements, or both. Conversely, the decline observed in Shaanxi and Gansu provinces could reflect the challenges posed by water scarcity, soil degradation, or policy shifts favoring less intensive farming practices [36,37].

At the national scale, from 2001 to 2023, we observed a trend that initially showed a decrease and then an increase in the percentages of multiple crops (see Figure 6). This pattern prompted us to conduct a further analysis for the period from 2013 to 2023, using the Mann–Kendall test and Sen's slope, to explore more recent trends. Within this timeframe, a subset of 3 km analytical windows exhibited either positive (n = 8400, or 3.13%) or negative (n = 5172, or 1.93%) trends, which were much fewer in comparison to the entire 2001 to 2023 period. One reason for this discrepancy is that the sample size for this time series analysis encompasses only 11 years, potentially limiting the detection of broader trends.

The 8-day MODIS NDVI datasets were found to offer sufficient temporal resolution for the large-scale mapping of cropping patterns. However, a limitation of this study was its focus on 'pure' cropland pixels at the 250 m spatial resolution. For MODIS pixels containing partial croplands, applying peak detection directly may lead to significant uncertainties due to interference from other land cover types, such as forests or urban areas, affecting the cropland's temporal signals [38]. A possible solution involves using spatial proximity to allocate cropping patterns based on neighboring pure croplands, where single or multiple crops can be mapped with greater accuracy. Furthermore, utilizing harmonized Landsat and Sentinel data [39] could facilitate the generation of 30 m resolution cropping pattern map products [31,40,41]. At the finer spatial resolution, the issue of land cover mixture can be substantially mitigated. In future studies, we plan to update our single-

and double-cropping map products by integrating continuous or dynamic land use/cover datasets for China, including CLCD [42] and CACD [43]. Future research should also consider the integration of additional data sources, including socio-economic datasets, to identify the driving factors behind the observed trends. Investigating the effects of policy changes and technological advancements on cropping practices could offer deeper insights into sustainable agricultural intensification and food security strategies in China and other regions.

5. Conclusions

This study focused on mapping large-scale annual cropping patterns using a peak detection algorithm applied to 8-day MODIS NDVI time-series data. Through the utilization of a calibration dataset, we employed a grid-search method to fine-tune the selection of parameters, such as the SG smoothing window size and peak width. Our results indicate that an SG moving window size of five to seven MODIS composites, coupled with a peak width of four MODIS composites, yielded the highest peak detection accuracy. Pixel-wise accuracy assessments for the mapping years of 2001, 2011, and 2021 showed good overall accuracy, ranging between 89.7% and 92.0%. Nationally, the percentage of multiple crops varied from 29.6% to 35.2% from 2001 to 2023. At a more granular level of 3 km analytical windows, approximately 12.9% exhibited significant changes, either positive or negative, as determined by the Mann–Kendall test and Sen's slope analyses. Notably, spatial clusters of both increasing and decreasing trends in cropping intensity were identified, particularly in the provinces of Hebei, Shandong, Shaanxi and Gansu, respectively. This medium-resolution annual cropping intensity data in China can be used to explore cropping potential, guide land use planning, adjust agricultural structure, estimate grain yield, and coordinate the food trade.

Author Contributions: Conceptualization, J.R. and Y.S.; methodology, J.R. and Y.S.; software, J.R. and Y.S.; validation, J.R., Y.S. and Y.W.; resources, J.R., Y.S. and Y.W.; data curation, J.R. and Y.S.; writing—original draft preparation, J.R. and Y.S.; writing—review and editing, J.R., Y.S. and Y.W.; visualization, J.R. and Y.S.; funding acquisition, J.R. and Y.S. All authors have read and agreed to the published version of the manuscript.

Funding: This research was funded by the National Natural Science Foundation of China (No. 41901231) and the Guangxi Science and Technology Major Program (No. AD23026180).

Data Availability Statement: The original contributions presented in the study are included in the article, further inquiries can be directed to the corresponding author.

Acknowledgments: We gratefully acknowledge Advanced Research Computing at Virginia Tech for providing computational resources that have contributed to the results reported within this paper. URL: https://arc.vt.edu/, accessed on 1 January 2020. The authors would like to thank the editor and reviewers for their constructive and insightful comments, which helped improve the quality of the paper. We also thank all data providers that have been used in this study.

Conflicts of Interest: The authors declare no conflict of interest.

References

1. Beets, W.C. *Multiple Cropping and Tropical Farming Systems*; CRC Press: Boca Raton, FL, USA, 2019.
2. Xu, J.; Gao, J.; de Holanda, H.V.; Rodríguez, L.F.; Caixeta-Filho, J.V.; Zhong, R.; Jiang, H.; Li, H.; Du, Z.; Wang, X.; et al. Double cropping and cropland expansion boost grain production in Brazil. *Nat. Food* **2021**, *2*, 264–273. [CrossRef] [PubMed]
3. Beillouin, D.; Ben-Ari, T.; Makowski, D. Evidence map of crop diversification strategies at the global scale. *Environ. Res. Lett.* **2019**, *14*, 123001. [CrossRef]
4. Waha, K.; Dietrich, J.P.; Portmann, F.T.; Siebert, S.; Thornton, P.K.; Bondeau, A.; Herrero, M. Multiple cropping systems of the world and the potential for increasing cropping intensity. *Glob. Environ. Chang.* **2020**, *64*, 102131. [CrossRef] [PubMed]
5. Gaba, S.; Lescourret, F.; Boudsocq, S.; Enjalbert, J.; Hinsinger, P.; Journet, E.P.; Navas, M.L.; Wery, J.; Louarn, G.; Malézieux, E.; et al. Multiple cropping systems as drivers for providing multiple ecosystem services: From concepts to design. *Agron. Sustain. Dev.* **2015**, *35*, 607–623. [CrossRef]

6. Ranck, E.J.; Holden, L.A.; Dillon, J.A.; Rotz, C.A.; Soder, K.J. Economic and environmental effects of double cropping winter annuals and corn using the Integrated Farm System Model. *J. Dairy Sci.* **2020**, *103*, 3804–3815. [CrossRef] [PubMed]
7. Xie, H.; Liu, G. Spatiotemporal differences and influencing factors of multiple cropping index in China during 1998–2012. *J. Geogr. Sci.* **2015**, *25*, 1283–1297. [CrossRef]
8. Yan, H.; Xiao, X.; Huang, H.; Liu, J.; Chen, J.; Bai, X. Multiple cropping intensity in China derived from agro-meteorological observations and MODIS data. *Chin. Geogr. Sci.* **2014**, *24*, 205–219. [CrossRef]
9. Li, S.; Li, X.; Sun, L.; Cao, G.; Fischer, G.; Tramberend, S. An estimation of the extent of cropland abandonment in mountainous regions of China. *Land Degrad. Dev.* **2018**, *29*, 1327–1342. [CrossRef]
10. Wang, Y.; Li, X.; Xin, L.; Tan, M. Farmland marginalization and its drivers in mountainous areas of China. *Sci. Total Environ.* **2020**, *719*, 135132. [CrossRef] [PubMed]
11. Lunetta, R.S.; Shao, Y.; Ediriwickrema, J.; Lyon, J.G. Monitoring agricultural cropping patterns across the Laurentian Great Lakes Basin using MODIS-NDVI data. *Int. J. Appl. Earth Obs. Geoinf.* **2010**, *12*, 81–88. [CrossRef]
12. Ren, J.; Campbell, J.B.; Shao, Y. Estimation of sos and eos for midwestern us corn and soybean crops. *Remote Sens.* **2017**, *9*, 722. [CrossRef]
13. Sakamoto, T.; Yokozawa, M.; Toritani, H.; Shibayama, M.; Ishitsuka, N.; Ohno, H. A crop phenology detection method using time-series MODIS data. *Remote Sens. Environ.* **2005**, *96*, 366–374. [CrossRef]
14. Shao, Y.; Lunetta, R.S.; Ediriwickrema, J.; Iiames, J. Mapping cropland and major crop types across the Great Lakes Basin using MODIS-NDVI data. *Photogramm. Eng. Remote Sens.* **2010**, *76*, 73–84. [CrossRef]
15. Zhu, X.; Li, Q.; Shen, M.; Chen, J.; Wu, J. A methodology for multiple cropping index extraction based on NDVI time-series. *J. Nat. Resour.* **2008**, *23*, 534–554.
16. Qiu, B.; Hu, X.; Chen, C.; Tang, Z.; Yang, P.; Zhu, X.; Yan, C.; Jian, Z. Maps of cropping patterns in China during 2015–2021. *Sci. Data* **2022**, *9*, 479. [CrossRef]
17. Yan, H.; Liu, F.; Qin, Y.; Doughty, R.; Xiao, X. Tracking the spatio-temporal change of cropping intensity in China during 2000–2015. *Environ. Res. Lett.* **2019**, *14*, 035008. [CrossRef]
18. Liu, X.; Zheng, J.; Yu, L.; Hao, P.; Chen, B.; Xin, Q.; Fu, H.; Gong, P. Annual dynamic dataset of global cropping intensity from 2001 to 2019. *Sci. Data* **2021**, *8*, 283. [CrossRef]
19. Ding, M.; Chen, Q.; Xin, L.; Li, L.; Li, X. Spatial and temporal variations of multiple cropping index in China based on SPOT-NDVI during 1999–2013. *Acta Geogr. Sin.* **2015**, *70*, 1080–1090.
20. Karra, K.; Kontgis, C.; Statman-Weil, Z.; Mazzariello, J.C.; Mathis, M.; Brumby, S.P. Global land use/land cover with Sentinel 2 and deep learning. In Proceedings of 2021 IEEE International Geoscience and Remote sensing Symposium (IGARSS), Brussels, Belgium, 11–16 July 2021; pp. 4704–4707.
21. Cui, Y.; Liu, R.; Li, Z.; Zhang, C.; Song, X.; Yang, J.; Yu, L.; Chen, M.; Dong, J. Decoding the inconsistency of six cropland maps in China. *Crop J.* **2024**, *12*, 281–294. [CrossRef]
22. Lunetta, R.S.; Knight, J.F.; Ediriwickrema, J.; Lyon, J.G.; Worthy, L.D. Land-cover change detection using multi-temporal MODIS NDVI data. In *Geospatial Information Handbook for Water Resources and Watershed Management*; CRC Press: Boca Raton, FL, USA, 2022; Volume II, pp. 65–88.
23. Shao, Y.; Lunetta, R.S.; Wheeler, B.; Iiames, J.S.; Campbell, J.B. An evaluation of time-series smoothing algorithms for land-cover classifications using MODIS-NDVI multi-temporal data. *Remote Sens. Environ.* **2016**, *174*, 258–265. [CrossRef]
24. Jönsson, P.; Eklundh, L. Seasonality extraction by function fitting to time-series of satellite sensor data. *IEEE Trans. Geosci. Remote Sens.* **2002**, *40*, 1824–1832. [CrossRef]
25. Gao, F.; Morisette, J.T.; Wolfe, R.E.; Ederer, G.; Pedelty, J.; Masuoka, E.; Myneni, R.; Tan, B.; Nightingale, J. An algorithm to produce temporally and spatially continuous MODIS-LAI time series. *IEEE Geosci. Remote Sens. Lett.* **2008**, *5*, 60–64. [CrossRef]
26. Liu, L.; Kang, S.; Xiong, X.; Qin, Y.; Wang, J.; Liu, Z.; Xiao, X. Cropping intensity map of China with 10 m spatial resolution from analyses of time-series Landsat-7/8 and Sentinel-2 images. *Int. J. Appl. Earth Obs. Geoinf.* **2023**, *124*, 103504. [CrossRef]
27. Sakamoto, T.; Van Nguyen, N.; Ohno, H.; Ishitsuka, N.; Yokozawa, M. Spatio–temporal distribution of rice phenology and cropping systems in the Mekong Delta with special reference to the seasonal water flow of the Mekong and Bassac rivers. *Remote Sens. Environ.* **2006**, *100*, 1–16. [CrossRef]
28. Yang, Y.; Ren, W.; Tao, B.; Ji, L.; Liang, L.; Ruane, A.C.; Fisher, J.B.; Liu, J.; Sama, M.; Li, Z.; et al. Characterizing spatiotemporal patterns of crop phenology across North America during 2000–2016 using satellite imagery and agricultural survey data. *ISPRS J. Photogramm. Remote Sens.* **2020**, *170*, 156–173. [CrossRef]
29. Murphy, K.P. *Machine Learning: A Probabilistic Perspective*; MIT Press: Cambridge, MA, USA, 2012.
30. Chen, Z.; Xu, C.; Ji, L.; Feng, J.; Li, F.; Zhou, X.; Fang, F. Effects of multi-cropping system on temporal and spatial distribution of carbon and nitrogen footprint of major crops in China. *Glob. Ecol. Conserv.* **2020**, *22*, e00895. [CrossRef]
31. Zhang, M.; Wu, B.; Zeng, H.; He, G.; Liu, C.; Tao, S.; Zhang, Q.; Nabil, M.; Tian, F.; Bofana, J.; et al. GCI30: A global dataset of 30-m cropping intensity using multisource remote sensing imagery. *Earth Syst. Sci. Data* **2021**, *13*, 4799–4817. [CrossRef]
32. Lu, M.; Wu, W.; You, L.; See, L.; Fritz, S.; Yu, Q.; Wei, Y.; Chen, D.; Yang, P.; Xue, B. A cultivated planet in 2010–Part 1: The global synergy cropland map. *Earth Syst. Sci. Data* **2020**, *12*, 1913–1928. [CrossRef]
33. Chai, J.; Wang, Z.; Yang, J.; Zhang, L. Analysis for spatial-temporal changes of grain production and farmland resource: Evidence from Hubei Province, central China. *J. Clean. Prod.* **2019**, *207*, 474–482. [CrossRef]

34. Hou, W.; Geng, T.; Chen, Q.; Chen, C. Impacts of climate warming on growth period and yield of rice in Northeast China during recent two decades. *Chin. J. Appl. Ecol.* **2015**, *26*, 249–259.
35. Jiang, M.; Li, X.; Xin, L.; Tan, M. The impact of paddy rice multiple cropping index changes in Southern China on national grain production capacity and its policy implication. *Acta Geogr. Sin.* **2019**, *74*, 32–43.
36. Qian, C.; Shao, L.; Hou, X.; Zhang, B.; Chen, W.; Xia, X. Detection and attribution of vegetation greening trend across distinct local landscapes under China's Grain to Green Program: A case study in Shaanxi Province. *Catena* **2019**, *183*, 1041. [CrossRef]
37. Zhang, Y.; Song, W.; Fu, S.; Yang, D. Decoupling of land use intensity and ecological environment in Gansu province, China. *Sustainability* **2020**, *12*, 2779. [CrossRef]
38. Shao, Y.; Lunetta, R.S. Sub-pixel mapping of tree canopy, impervious surfaces, and cropland in the Laurentian Great Lakes Basin using MODIS time-series data. *IEEE J. Sel. Top. Appl. Earth Obs. Remote Sens.* **2011**, *4*, 336–347. [CrossRef]
39. Claverie, M.; Ju, J.; Masek, J.G.; Dungan, J.L.; Vermote, E.F.; Roger, J.C.; Skakun, S.V.; Justice, C. The Harmonized Landsat and Sentinel-2 surface reflectance data set. *Remote Sens. Environ.* **2018**, *219*, 145–161. [CrossRef]
40. Gao, F.; Zhang, X. Mapping crop phenology in near real-time using satellite remote sensing: Challenges and opportunities. *J. Remote Sens.* **2021**, *1*, 96–109. [CrossRef]
41. Shao, Y.; Ren, J.; Campbell, J.B. Multitemporal Remote Sensing Data Analysis for Agricultural Application. *Compr. Remote Sens.* **2018**, *9*, 29–38.
42. Yang, J.; Huang, X. The 30 m annual land cover dataset and its dynamics in China from 1990 to 2019. *Earth Syst. Sci. Data* **2021**, *13*, 3907–3935. [CrossRef]
43. Tu, Y.; Wu, S.; Chen, B.; Weng, Q.; Bai, Y.; Yang, J.; Yu, L.; Xu, B. A 30 m annual cropland dataset of China from 1986 to 2021. *Earth Syst. Sci. Data* **2024**, *16*, 2297–2316. [CrossRef]

Disclaimer/Publisher's Note: The statements, opinions and data contained in all publications are solely those of the individual author(s) and contributor(s) and not of MDPI and/or the editor(s). MDPI and/or the editor(s) disclaim responsibility for any injury to people or property resulting from any ideas, methods, instructions or products referred to in the content.